

# Modulation-Based Simultaneous Wireless Information and Power Transfer

Akashkumar Rajaram<sup>1</sup>, Dushantha Nalin K. Jayakody<sup>2</sup>, Senior Member, IEEE, Bin Chen<sup>3</sup>, Member, IEEE, Rui Dinis<sup>4</sup>, Senior Member, IEEE, and Sofiène Affes<sup>5</sup>, Senior Member, IEEE

**Abstract**—Due to the rapid growth of IoT and other connected devices, developing battery-less and/or self-sustainable devices to enable green communication is crucial. This letter presents a practical simultaneous wireless information and power transfer (SWIPT) scheme based on an  $M$ -ary quadrature-amplitude modulation (QAM) modulation based technique ( $MS$ ). The proposed scheme employs hybrid constellation shaping system (HCS) to improve the spectral efficiency. We compare  $MS$  with the traditional power splitting scheme based SWIPT ( $PS$ ) technique. We demonstrate that our proposed scheme outperforms  $PS$  in terms of the error rate performance.  $MS$  scheme is mainly focused on improving the reliability of low powered IoT sensors and it offers better achievable information rate at operating SNR region as compared to that of  $PS$ . Those improvements come at the expense of a slight reduction in the maximum achievable spectral efficiency.

**Index Terms**—Hybrid constellation shaping,  $M$ -QAM modulation, simultaneous wireless information and power transfer.

## I. INTRODUCTION

ENERGY harvesting (EH) in wireless communication networks is one of the enabling technologies for future generation networks [1]. EH is a green communication scheme for harvesting energy from radio frequency (RF) signals [2]. In [3], researchers investigated the performance of simultaneous wireless information and power transfer (SWIPT) adopting an  $M$ -ary modulation scheme, which represents a major leap

Manuscript received June 26, 2019; revised August 19, 2019; accepted September 24, 2019. Date of publication October 8, 2019; date of current version January 8, 2020. This work is funded, in part, by the Competitive Enhancement Program by Tomsk Polytechnic University, Russia. B. Chen is supported by the National Natural Science Foundation of China (NSFC) under Grant 61701155 and Fundamental Research Funds for the Central Universities under Grant JZ2019HGBZ0130. This work was also supported by Fundação para a Ciência e Tecnologia and Instituto de Telecomunicações under projects UID/EEA/50008/2019 and MASSIVE5G (SAICT-45-2017-02). The associate editor coordinating the review of this letter and approving it for publication was Q. Wu. (Corresponding author: Dushantha Nalin K. Jayakody.)

A. Rajaram is with the Department of Electrical and Computer Engineering, Faculty of Science and Technology, New University of Lisbon, 2829-516 Caparica, Portugal, with the Instituto de Telecomunicações, 1049-001 Lisbon, Portugal, and also with the School of Computer Science & Robotics, National Research Tomsk Polytechnic University, 634050 Tomsk, Russia (e-mail: a.rajaram@campus.fct.ul.pt).

D. N. K. Jayakody is with Sri Lanka Technological Campus, Padukka 10500, Sri Lanka, and also with the School of Computer Science & Robotics, National Research Tomsk Polytechnic University, 634050 Tomsk, Russia (e-mail: nalin.jayakody@ieee.org).

B. Chen is with the Department of Computer Science and Information Engineering, Hefei University of Technology, Hefei 230000, China, and also with the Department of Electrical Engineering, Eindhoven University of Technology, 5612 AZ Eindhoven, The Netherlands (e-mail: chen.bin.conan@gmail.com).

R. Dinis is with the Department of Electrical and Computer Engineering, Faculty of Science and Technology, New University of Lisbon, 2829-516 Caparica, Portugal, and also with the Instituto de Telecomunicações, 1049-001 Lisbon, Portugal (e-mail: rdinis@fct.unl.pt).

S. Affes is with INRS, Montreal, QC H5A 1K6, Canada (e-mail: affes@emt.inrs.ca).

Digital Object Identifier 10.1109/LCOMM.2019.2946236

forward as it does not require a dedicated beam as in the case of wireless power transfer. However, this comes at the expense of some loss in the system throughput since part of the transmitted signal is used for power transfer. Furthermore, EH is beneficial only when the received signal power is greater than a certain sensitivity level.

In this letter, we introduce a new SWIPT scheme called modulation-based SWIPT ( $MS$ ), which involves using specific constellation points (CPs) for EH and the remaining ones for information transmission (IT). This suggests that the CPs intended for IT do not suffer direct power loss due to EH, which is different from how CPs are used in traditional power splitting and time switching architectures [1], [2]. However in  $MS$ , the excess amount of energy will be spent in transmitting symbols for EH. Alternatively, symbols carrying information and energy can be transmitted in two separate signal streams using two different time slots, but this consumes excess time resource, decreasing the spectral efficiency [1]. Due to the nature of CPs usage in  $MS$ , it gives us an opportunity to shape the CPs to improve the performance of  $MS$ . The idea of shaping the CPs is introduced in [4] and their performance is studied in [5] and [6]. We can improve the spectral efficiency of  $MS$  by utilizing hybrid constellation shaping (HCS) [7] and in  $MS$ , HCS of  $M$ -ary modulation is adopted. HCS is a hybrid geometric and probabilistic shaping method that modifies the nature of the signal to a non-uniform and non-equidistant constellation point distribution. HCS is preferred over geometric shaping (GS) and probabilistic amplitude shaping (PAS) as it maintains the total amount of energy of each constellation point (CP) like regular  $M$ -QAM. This helps in allocating fixed amounts of energies for IT and EH, regardless of the degree of constellation shaping.

In contrast with existing SWIPT techniques, we show that  $MS$  has better Symbol error rate (SER) and maximum achievable information rate (AIR) for low signal-to-noise ratio (SNR) operating region. However, at high SNR, the AIR of  $MS$  does not reach its the maximum rate due to the fact that some CPs are used for EH. AIR of  $MS$  can be further improved for certain SNR region by using HCS. Thus, HCS is effective for our proposed  $MS$  scheme to improve AIR as compared to using a regular  $M$ -QAM scheme for EH and IT.

## II. SYSTEM MODEL

We assume a point-to-point communication system comprising a transmitter  $S$  and a receiver  $D$ . The input signal  $\mathbf{x}$  is transmitted by using the transmit power  $P_T$  over Rayleigh fading channel and the channel co-efficient is given as  $h$ , where  $h \sim CN(0, \sigma^2)$  and the channel power gain is  $|h|^2$ , which has an exponential distribution. The channel noise  $\mathbf{n}$  is additive white Gaussian noise (AWGN) with zero mean and variance  $\sigma_{SD}^2$ ,  $\mathbf{n} \sim N(0, \sigma_{SD}^2) = N(0, N_0/2)$ .  $\mathbf{x}$  has  $K$  symbols and the  $k$ th individual symbols of  $\mathbf{x}$  are denoted by

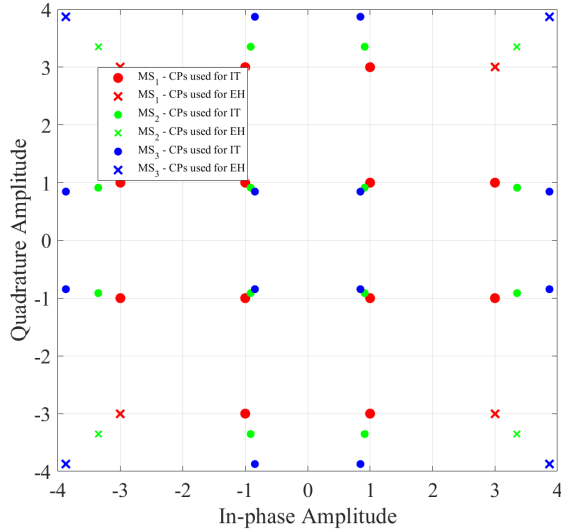


Fig. 1. The CPs of  $MS_1$ ,  $MS_2$  and  $MS_3$  are illustrated without considering their respective per symbol transmit power. The models are described in Sec. III and its alphabets are mentioned in Tab. I. The HCS of  $MS_3$  model is illustrated in Fig. 2.

$x^{[k]}$ ,  $k = 1, \dots, K$ .<sup>1</sup> The CPs of  $\mathbf{x}$  are based on a square  $M$ -QAM modulation, where  $M = 2^b$ , and  $b$  is the number of bits per symbol. CPs are denoted as  $A^{[s]}$ , where  $s$  is the index of CP, with  $s = 1, \dots, M$ .

#### A. Modulation-Based SWIPT Technique

In the  $MS$ , all the highest energy CPs (with same magnitude) are selected for EH and are denoted by the set  $A_e^{[s]}$ . The rest of the CPs are used for IT, and define the set  $A_i^{[s]}$ . Here,  $\{A_e^{[s]}, A_i^{[s]}\} \in A^{[s]}$  and  $MS$  are illustrated in Fig. 1. If  $x^{[k]} \in A_e^{[s]}$ , then it is denoted as  $x_e^{[k]}$ , else it is denoted as  $x_i^{[k]}$ . Here,  $x_i^{[k]}$  and  $x_e^{[k]}$  are orderly positioned in a pattern known to  $S$  and  $D$ , and based on this pattern and amplitude of the symbols, the receiver separates the symbols for IT and EH.

The basis of selecting CPs for EH in  $M$ -QAM is dependant on two factors. Firstly, the amount of energy to be harvested. Since each constellation point have a fixed amount of energy level, the fraction of CPs for EH can be used to select to select the desired energy ratio between EH and IT. Secondly, while choosing the CPs for EH,  $A_e^{[s]}$ , if high amplitude CPs are chosen for EH and other CPs for IT, then it will be comparatively easy for the receiver to distinguish specific symbols for IT and this simplifies the receiver synchronization between EH and IT. Moreover, the EH signal should be designed to avoid undesirable spectral lines, which is achieved with a pseudo-random selection within  $A_e^{[s]}$  and a set  $A_e^{[s]}$  with zero mean (that is the case of the set of higher energy CPs in a QAM constellation).

$$\mathbf{y} = \sqrt{\frac{P_T}{E_M}} h \mathbf{x} + \mathbf{n}, \quad (1)$$

where  $E_M$  is the average amount of energy of the symbol and  $P_T$  is the transmit power. The amount of energy harvested from the received signal at  $D$  is given as

$$E_D = \frac{\eta_{EH} P_T |h|^2 \vartheta}{d_{SD}^{-\Psi}}, \quad (2)$$

<sup>1</sup>In this letter, irrespective index  $k$  of the symbol, only the set of symbols used for IT is considered for calculating SER and AIR performance.

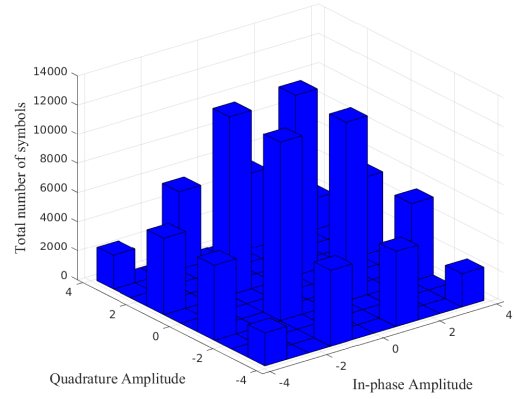


Fig. 2. The symbols distributed across the CPs of 16-QAM signal based on HCS model  $B_3$  is described in Sec. III and its alphabets are mentioned in Tab. I.

where  $\eta_{EH}$  is the RF energy harvesting efficiency, the distance between  $S$  and  $D$  is denoted as  $d_{SD}$  and  $\Psi$  is the path loss factor.  $\vartheta = E_e/E_S$ ,  $E_e$  and  $E_S$  are the total amount of energy present in  $\mathbf{x}_e$  and  $\mathbf{x}$ , respectively and  $T$  is the time taken for transmitting  $\mathbf{x}$ .  $E_e$  and  $E_S$  are given as  $E_e = \mathbb{E}[|\mathbf{x}_e|^2]$  and  $E_S = \mathbb{E}[|\mathbf{x}|^2]$ , respectively.<sup>2</sup> The transmit SNR of  $\mathbf{x}$  is denoted as  $\gamma$  and  $\gamma = \frac{E_S}{N_0}$ .

#### B. Hybrid Constellation Shaping in $M$ -QAM

HCS shapes the CPs by changing the amplitude and probability of occurrence of the symbols of each CP and thereby changes the percentage of symbols present in each CP and the amplitude of respective symbols. HCS model is illustrated in Fig. 2<sup>3</sup> and in Fig. 1. An important feature of HCS is that irrespective of the degree of shaping, the total amount of energy in each CP is constant.  $A^{[s]}$  is represented in a complex form by the combination of the individual alphabets, where the alphabets are denoted as  $a$ , where  $a$  in real and imaginary axis are denoted as  $a$  and  $ja$ , respectively. The value of  $a$  is  $(2m-1)$ , where if  $M \geq 16$  then  $m = 1, \dots, \frac{\sqrt{M}}{2}$ , or else if  $M = 4$ , then  $m = 1$ . The value of  $A^{[s]}$  due to HCS is expressed as

$$A^{[s]} = \pm \frac{\rho_u(a)}{\rho(a)} a \pm \frac{\rho_u(ja)}{\rho(ja)} ja, \quad (3)$$

where the non-uniform probability and uniform probability occurrences of  $a$  in CPs are denoted as  $\rho(a)$  and  $\rho_u(a)$ , respectively. Similarly, the non-uniform probability and uniform probability occurrence of  $ja$  in CPs are denoted as  $\rho(ja)$  and  $\rho_u(ja)$ , respectively. To validate perfect HCS of  $M$ -QAM signal, the signal stream  $x^{[k]}$  belonging to  $A^{[s]}$  should satisfy the following condition.

$$\mathbb{E}\left[\pm \frac{\rho_u(a)}{\rho(a)} a \pm \frac{\rho_u(ja)}{\rho(ja)} ja\right] = \mathbb{E}[\pm \rho_u(a) ja \pm \rho_u(ja) ja], \quad (4)$$

where (4) is a condition in which, the expected value of individual CP with HCS as in (3) should always be equal to the expected value of its respective CP with uniform symbol distribution.

#### C. Comparison of $MS$ and $PS$

The  $MS$  is compared with the traditional power splitting scheme based SWIPT ( $PS$ ). Both  $MS$  and  $PS$  schemes divide

<sup>2</sup>The expected value operator is denoted as  $\mathbb{E}[w]$ , where  $w$  is a variable.

<sup>3</sup>For our convenience, only  $B_3$  model is illustrated.

the transmit power for EH and information decoding (ID) but the method of dividing the power is different for both the schemes. In *PS*, energy is harvested from  $\mathbf{y}$  by using a power splitting circuit and this circuit divides the power of the signal for EH and information decoding [1], [2]. Thus, in *PS* all the symbols are used for EH, whereas in *MS*, EH only from the specific CPs of  $\mathbf{y}$ . In *MS*, the total number of symbols used for IT and EH are denoted as  $N_i$  and  $N_e$ , respectively.  $N_i$  should be equal in both *MS* and *PS*, and then  $K = N_i/(100 - \rho(\mathbf{x}_e))\%$ , where  $\rho_u(\mathbf{x}_e)$  is the probability of  $x_e$  present in  $\mathbf{x}$  and  $N_e = N - N_i$ . Irrespective of additional symbols present in *MS*,  $N_i$  should be equal in both *MS* and *PS* and also  $P_T$  should be equal in both *PS* and *MS* to compare both the EH schemes. The transmit power used in *MS* for each symbol is given as

$$P_m = P(N_i/(N_e + N_i)), \quad (5)$$

where  $P$  is the transmit power of each symbol present in *PS*.

The SER performance of *MS* and *PS* models are dependant on SNR condition and minimum distance between  $\mathbf{x}_i$  and its neighboring symbol, which is denoted as  $d_{x_i^{[k]}}$ .  $d_{x_i^{[k]}}$  of both the schemes are dependant on the position of CPs and the power allocated for the symbols to perform IT. In uniform CPs distribution, the relationship between *MS* and *PS* in terms of  $d_{x_i^{[k]}}$  and transmit power per symbol is given as

$$P_m d_{x_i^{[k]}} = \alpha P d_{x_i^{[k]}}, \quad (6)$$

where  $\alpha$  is the fraction of  $P$  allocated for IT and the value of  $d_{x_i^{[k]}}$  varies depending on HCS models. The minimum distance of a 16-QAM signal using *MS* and *PS* models with equal number for symbols for IT and also with equal value of  $P_T$  are illustrated in Fig. 3. The figure shows that  $d_{x_i^{[k]}}$  in *MS* is greater than that of *PS*. Also by using HCS, it is possible to increase  $d_{x_i^{[k]}}$  of symbols in *MS*. Fig. 3 illustrates  $d_{x_i^{[k]}}$  of  $MS_1$  and  $MS_3$  and the value is calculated in Tab. I. As compared to  $MS_1$ , in  $MS_3$ , the HCS reduces the amplitude of symbols in low amplitude CPs and increases the amplitude of symbols in high amplitude CPs and this decreases  $N_e$  of  $MS_3$  over  $MS_1$ , thus  $P_m$  increases with the decrease  $N_e$ .

The basis of selecting the degree of HCS is dependant on the operating SNR region of the system and Shannon entropy of the signal, which is denoted as  $H(\mathbf{x})$ . For different operating SNR region, the system can be adapted by adjusting  $P_m$  value with the change in the degree of HCS.  $H(\mathbf{x})$  is maximum under uniform HCS. For a regular  $M$ -QAM signal with uniform probability occurrence of CPs,  $H(\mathbf{x}) = \sum_{s=1}^M \rho_u(A_i^{[s]}) \log(1/\rho_u(A_i^{[s]}))$ , where  $\rho_u(A_i^{[s]})$  is the uniform probability of symbols belonging to  $A_i^{[s]}$  is present in  $\mathbf{x}$ . Similarly, for  $M$ -QAM signal with HCS, we should considered only the CPs used for IT. Also, the percentage of excess symbols used in  $A_i^{[s]}$  should be considered in calculating Shannon entropy of *MS* and it is given as

$$H(\mathbf{x}_i) = \sum_{s=1}^M \left( \rho(A_i^{[s]}) \frac{N_e + N_i}{N_i} \right) \log \left( \frac{\{\rho(A_i^{[s]})\}^{-1}}{\frac{N_e + N_i}{N_i}} \right), \quad (7)$$

here  $(N_e + N_i)/N_i$  is the percentage of increase in the symbols belonging to  $A_i^{[s]}$  and  $\rho(A_i^{[s]})$  is the non-uniform

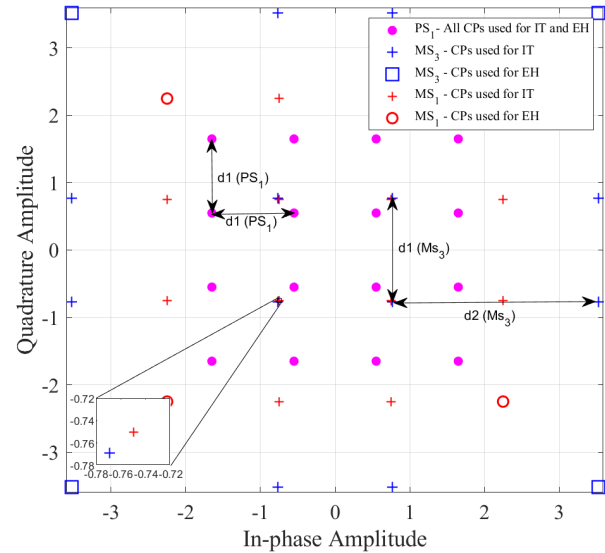


Fig. 3. The minimum distance between CPs of  $MS_1$ ,  $MS_3$  and  $PS_1$  are illustrated as given in Tab. II. Note that the position of CPs in *MS* scheme varies when compared to their respective position illustrated in Fig. 1 because of the consideration of their respective  $P_m$ .

probability of symbols belonging to  $A_i^{[s]}$  is present in  $\mathbf{x}$ . Even though  $N_i$  is equal for both the regular signal and *MS* signal,  $H(\mathbf{x})$  decreases with the decrease in randomness. AIR of *MS* signal is denoted as  $A_M$ . The maximum  $A_M$  of the signal is determined by the value of  $H(\mathbf{x}_i)$  and it is also necessary to select HCS models based on its  $H(\mathbf{x}_i)$  value and operating SNR region where the maximum  $A_M$  can be achieved.

In general, *PS* should have better AIR performance than that of *MS* due to the usage of all the CPs of regular  $M$ -QAM signal and uniform CPs distribution. In *PS*, due to the fact that the energy is harvested from all the symbols in the signal, the SNR of the symbols in low amplitude CPs suffers energy loss as opposed to the case of low amplitude symbols in *MS* and it is illustrated in Fig. 3. Thus, at low SNR, the HCS models in combination with *MS* having low  $H(\mathbf{x})$  can possibly perform better than the models with high  $H(\mathbf{x})$  value.

#### D. Theoretical Symbol Error and Achievable Rate of $M$ -QAM With *MS*

In this section, average SER is derived for the proposed system using  $M$ -QAM signal with HCS. The symbols of  $M$ -QAM are located in three regions of CPs. There are 4 symbols in the corner,  $4(\sqrt{M} - 2)$  symbols on the edge of CPs and  $(\sqrt{M} - 2)^2$  symbols in the interior. The approximated SER of individual symbols located in corner, edges and interior is  $2\xi_{Cr}$ ,  $3\xi_{Ed}$  and  $4\xi_{In}$ , respectively. The SER of an individual symbol is denoted as  $\xi_{x_i}$ . Depending on the location of symbols in the constellation map,  $\xi_{x_i} \subset \{\xi_{Cr}, \xi_{Ed}, \xi_{In}\}$ . Thus,  $\xi_{x_i}$  is given as

$$\begin{aligned} \xi_{x_i} &= \int_0^\infty Q(2d_{x_i^{[k]}} a_h \gamma) 2a_h e^{-(a_h^2)} da_h \\ &= \frac{1}{2} \left( 1 - \sqrt{\frac{d_{x_i^{[k]}} \gamma}{1 + d_{x_i^{[k]}} \gamma}} \right), \end{aligned} \quad (8)$$

where  $a_h$  is amplitude of the channel  $h$  and  $da_h$  is the differential of  $a_h$ . The neighboring CPs are used for either IT or EH. In case of 4-QAM, all the symbols are considered as the corner symbols. Thus, depending on the energy requirement, the symbols in 4-QAM are used for either EH or IT.

The average SER of  $MS$  signal is derived based on the general SER of  $M$ -QAM signal derivation in [8] but it varies from the SER of  $M$ -QAM signal due to non-uniform constellation shaping,  $d_{x_i^{[k]}}$  of  $x_i^{[k]}$ , and  $A_i^{[s]}$ . The  $d_{x_i^{[k]}}$  of  $x_i^{[k]}$  is considered based on the closest neighboring CPs. In the case of communication error, the probability of  $x_i^{[k]}$  occurring in CPs other than the closest neighboring CP region is not considered. If  $\mathbf{x}_i$  moves towards the direction of other neighboring CPs region apart from the closest neighboring CP region, then the possibility of error decreases due to the increase in  $d_{x_i^{[k]}}$ . Hence, this is an upper bound SER for the  $M$ -QAM with non-uniform HCS. The SER for individual symbol present in  $x_i^{[k]}$  is given as

$$\xi_M[x_i^{[k]}] \approx \begin{cases} 3\xi_{Ed}, & x_i^{[k]} = \left\{ \pm \frac{\rho_u(a)}{\rho(a)} a \pm j1 \frac{\rho_u(ja)}{\rho(ja)} \right\} \\ 3\xi_{Ed}, & x_i^{[k]} = \left\{ \pm 1 \frac{\rho_u(a)}{\rho(a)} \pm ja \frac{\rho_u(ja)}{\rho(ja)} \right\} \\ 4\xi_{In}, & x_i^{[k]} = \left\{ \pm \frac{\rho_u(a)}{\rho(a)} (2m_i - 1) \right. \\ & \left. \pm j \frac{\rho_u(ja)}{\rho(ja)} (2m_i - 1) \right\}, \end{cases} \quad (9)$$

where if  $M = 16$ , then  $m_i = 1$  or else if  $M > 16$ , then  $m_i = \{1, \dots, \frac{\sqrt{M}}{2} - 1\}$  and the SER of symbols in corner CPs are not considered in  $\xi_M[x_i^{[k]}]$ . The average SER of all the symbols present in  $\mathbf{x}_i$  gives the SER of  $MS$  signal and it is given as  $\xi_M \approx \frac{1}{K} \sum_{k=1}^K \xi_M[x_i^{[k]}]$ .

The maximum AIR is one of the performance metrics which is considered for understanding the feasibility of  $MS$ , since it uses the highest amplitude symbols for EH. The symbol-wise mutual information between input and output symbols of a signal in a finite auxiliary channel with Monte Carlo integration is given in [9, Sec. VI]. This formula is used to find an approximate lower bound AIR for the signal with PAS by using circularly symmetric Gaussian noise statistics as in [10]. The benefit of using Monte Carlo simulation based equation is that the impact of HCS of the given input signal is considered in estimating its AIR. Therefore, as similar to AIR of PAS, an approximate lower bound AIR for the signal with HCS can be estimated by using [10, Eq.5]. The AIR of  $MS$  is given as

$$A_M \approx \frac{1}{K} \sum_{k=1}^K \log_2 \frac{Q_{\mathbf{y}|\mathbf{x}_i}(\mathbf{y}^{[k]}|x_i^{[k]})}{Q_{\mathbf{y}}(\mathbf{y}^{[k]})}, \quad (10)$$

where  $\mathbf{y}^{[k]}$  is the output symbol corresponding to the input symbol  $x_i^{[k]}$ , and  $k = 1, \dots, K$ . Here,  $Q_{\mathbf{y}|\mathbf{x}_i}$  and  $Q_{\mathbf{y}}$  denotes the auxiliary channel and the auxiliary channel output density, respectively. It is assumed that the transition probability distribution of  $Q_{\mathbf{y}|\mathbf{x}_i}$  is same as  $h$ .  $Q_{\mathbf{y}|\mathbf{x}_i}(\mathbf{y}^{[k]}|x_i^{[k]})$  and  $Q_{\mathbf{y}}(\mathbf{y}^{[k]})$  are derived in [10].

### III. NUMERICAL RESULTS

In this section, four HCS models are presented with  $MS$  scheme and they are compared with  $PS$  to find the best  $MS$

TABLE I  
PROBABILITY AND AMPLITUDE OF THE ALPHABETS,  $d_{x_i^{[k]}}$  OF THE ALPHABETS IN  $B_j$  AND  $H(\mathbf{x})$  OF  $B_j$

$B_j$	$\rho(a)$	$a$	$d_{x_i^{[k]},H}$	$d_{x_i^{[k]},L}$	$H(\mathbf{x})$
$B_1$	{0.25, 0.25}	{ $\pm 3, \pm 1$ }	2	2	4
$B_2$	{0.20, 0.30}	{ $\pm 3.3541, \pm 0.9129$ }	2.44	1.83	3.9419
$B_3$	{0.15, 0.35}	{ $\pm 3.8730, \pm 0.8452$ }	3.03	1.69	3.7626
$B_4$	{0.10, 0.40}	{ $\pm 4.7434, \pm 0.7906$ }	3.95	1.58	3.4439

TABLE II  
EH MODELS AND  $B_j$  OF THE RESPECTIVE EH MODELS,  $d_{x_i^{[k]},L}$  OF THE ALPHABETS IN EH MODELS,  $H(\mathbf{x}_i)$  OF  $MS_j$ ,  $N_i$ , AND  $K$  OF EH MODELS

models	$B_j$	$d_{x_i^{[k]},L}$	$H(\mathbf{x}_i)$	$N_i$	$K$
$MS_1$	$B_1$	$2 \times 0.75 = 1.5$	3.5850	$10^6$	$10^6(100/75)$
$MS_2$	$B_2$	$1.83 \times 0.86 = 1.54$	3.5567	$10^6$	$10^6(100/84)$
$MS_3$	$B_3$	$1.69 \times 0.92 = 1.55$	3.4573	$10^6$	$10^6(100/91)$
$MS_4$	$B_4$	$1.58 \times 0.96 = 1.52$	3.2516	$10^6$	$10^6(100/96)$
$PS_{\alpha 1}$	$B_1$	$2 \times 0.55 = 1.1$	4	$10^6$	$10^6$

scheme. Four HCS models are used over a 16-QAM signal, as shown in Tab. I with 0.05% variation in  $\rho(a)$  between each model and they are named as  $B_j$  where  $j = 1, 2, 3, 4$  and we consider  $\rho(a)$  and  $\rho(ja)$  are equal and the amplitude of  $a$  and  $ja$  are equal. These four HCS models are applied<sup>4</sup> on  $MS_j$ . We gradually vary  $\rho(a)$  in  $B_j$  to understand the impact of  $\rho(a)$  in the performance of  $MS_j$ . In the 16-QAM signal,  $x_{A3}^{[k]} = (\pm 3(\frac{\rho_u(a)}{\rho(a)}), \pm 3j(\frac{\rho_u(ja)}{\rho(ja)}))$ , where  $x_H^{[k]}$  denotes the highest amplitude symbols.  $d_{x_i^{[k]}}$  for  $x_H^{[k]}$  is denoted as  $d_{x_i^{[k]},H}$  and for the remaining CPs,  $d_{x_i^{[k]}}$  is denoted as  $d_{x_i^{[k]},L}$ .  $B_1$  is equal to  $\rho_u(a)$ .  $B_2, B_3$  and  $B_4$  models has non-uniform probability distribution of  $a$  and their respective bit energy value is calculated by using (3) as shown in Tab. I.  $MS_j$  uses  $x_H^{[k]}$  for EH and the rest of the CPs for IT.  $MS_1, MS_2, MS_3$  and  $MS_4$  uses 25%, 16%, 9% and 4% symbols for EH, respectively. At condition ideal,  $E_D$  of  $MS_j$  is constant with  $\vartheta = 45\%$ . For fair comparison of EH schemes,  $PS$  uses  $B_1$  with  $(1 - \alpha) = 45\%$  and it is denoted as  $PS_{\alpha 1}$ . For the energy harvesting simulation set-up,  $d_{SD}$  varies from 1 m to 5 m. It is assumed that  $\Psi = 2$ ,  $\eta_{EH} = 0.9$ ,  $P_T = 50$  dBm,  $T = 1$  second and the signal attenuation is constant at 30 dBm. EH at  $MS_j$  and  $PS_{\alpha 1}$  are equal as both the schemes allocate on 45% power for EH.  $E_D = 0.036, 0.009, 0.004, 0.002$  and  $0.0015$  at  $d_{SD} = 1, 2, 3, 4$  and 5, respectively.  $E_D$  decreases with the increase in distance due to path loss factor.

Tab. II illustrates  $d_{x_i^{[k]},L}$  of the alphabets in EH Models,  $H(\mathbf{x}_i)$  of  $MS_j$  and  $N_i, N_e$ , and  $K$  of EH models.  $d_{x_i^{[k]},L}$  is calculated for  $MS_j$  and  $PS_{\alpha 1}$  by using (5), (6) and  $d_{x_i^{[k]},L}$  of  $B_j$  from Tab. I.  $d_{x_i^{[k]},H}$  is not considered as  $x_H^{[k]}$  is not used for IT and for  $PS_{\alpha 1}$ ,  $d_{x_i^{[k]},H} = d_{x_i^{[k]},L}$ . For  $MS_3$ ,  $d_{x_i^{[k]},L} = 1.69 \times 0.917 = 1.55$ , where  $d_{x_i^{[k]},L}$  of  $B_3$  is 1.69 and  $P_m$  of  $x_i^{[k]}$  is 91.7%. In case of  $PS_{\alpha 1}$ ,  $d_{x_i^{[k]},H} = d_{x_i^{[k]},L}$  for  $B_1$

<sup>4</sup>In this section, for convenience, we use notation  $MS_j$  to denote the subcategory of  $MS$  scheme.

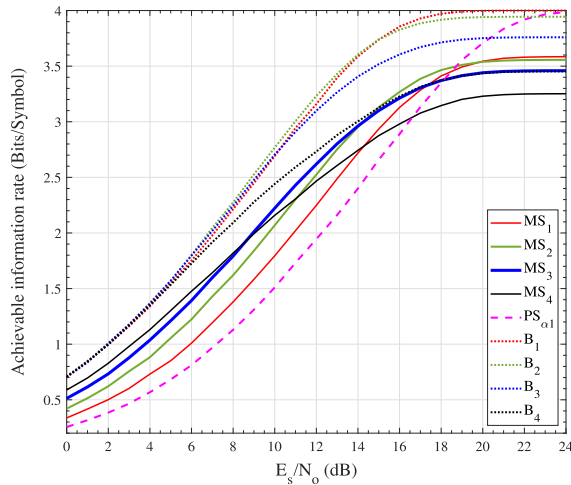


Fig. 4. A comparison between AIR of  $MS_j$  and  $PS_{\alpha 1}$ .

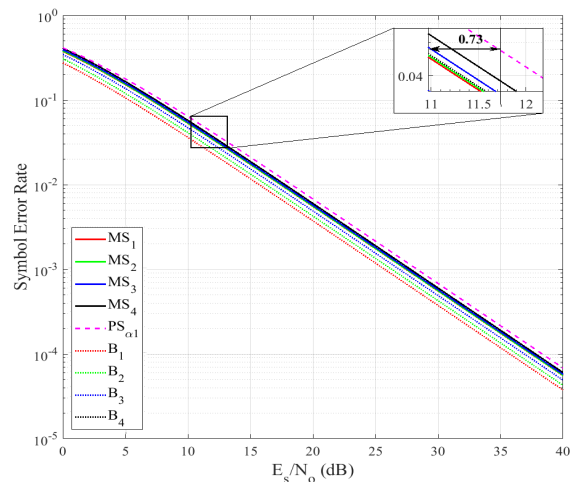


Fig. 5. A comparison between SER of  $MS_j$  and  $PS_{\alpha 1}$ .

model and  $d_{x_i^{[k]}}^1 = 2 \times 0.75 = 1.50$ , where  $d_{x_i^{[k]},L}$  of  $B_1$  is 2 and  $P$  of  $x_i^{[k]}$  is 75%. Similarly,  $d_{x_i^{[k]},L}$  of symbols in  $MS_j$  are calculated.

To analyse SER and AIR performance of  $MS_j$  and  $PS_{\alpha 1}$ , we set  $P_T = 1$  and the distance is not considered in this set-up. Fig. 4 illustrates the AIR of  $MS_j$  and  $B_j$ , and  $PS_{\alpha 1}$ . In general, the AIR performance is in the order of  $B_1 > B_2 > B_3 > B_4$  with the increase in non-uniform HCS. For SNR region from 0 dB to 16.5 dB, all  $MS_j$  performs better than  $PS_{\alpha 1}$  and particularly the performance improves with the increase in degree of HCS because in  $MS_j$  other than the  $x_H^{[k]}$  symbols,  $x_i^{[k]}$  does not suffer energy loss. Also the amount of energy loss of  $x_i^{[k]}$  is comparatively lesser in  $MS_j$  with the increase in degree of HCS. At any SNR greater than 7 dB,  $PS_{\alpha 1}$  performs better than  $MS_j$  because  $MS_j$  does not use  $x_H^{[k]}$  symbols for IT. After 20 dB SNR,  $MS_j$  saturates at its respective  $H(\mathbf{x}_i)$  as illustrated in Tab. II. While considering a broader operating SNR region in Fig. 4 i.e. from 0 dB to 15 dB SNR,  $MS_3$  performs better than  $MS_j$  and  $PS_{\alpha 1}$  until 15 dB and 18 dB SNR, respectively.  $MS_3$  has a SNR gain in

the range of 1.5 dB to 3.5 dB over  $PS_{\alpha 1}$  from 0 dB to 16 dB SNR.

Fig. 5 illustrates upper bound SER of  $MS_j$  and  $B_j$ , and the SER of  $PS_{\alpha 1}$ . In general, the SER performance is in the order of  $B_1 > B_2 > B_3$  because higher order modulated symbols and  $d_{x_i^{[k]}}$  is in the order of  $B_1 > B_2 > B_3$  as in Tab. I. The performance of  $MS_j$  as compared to that of  $B_j$  shows that SER does not change within  $MS_j$  as like in  $B_j$ , this is due to similar  $d_{x_i^{[k]}}$  as result of power compensation which is illustrated in Tab. II and fig. 3. Performance within EH schemes shows that, the performance of  $MS_j$  is better due to less amount of energy loss for  $x_i^{[k]}$ . Both Tab. II and Fig. 3 illustrate that  $d_{x_i^{[k]},L}$  of  $MS_j$  is better than  $PS_{\alpha 1}$  and,  $d_{x_i^{[k]},L}$  of  $MS_3$  is better than  $MS_1$  as explained in Sec. II-C. Therefore by considering  $d_{x_i^{[k]},L}$  of  $MS_3$  and  $PS_{\alpha 1}$ , even with the same power allocation for EH, at 11 dB SNR, the difference in  $d_{x_i^{[k]}}$  helps  $MS_3$  to outperform  $PS_{\alpha 1}$  by around 1 dB SNR gain.

#### IV. CONCLUSION

In this letter, we introduced a new SWIPT technique described as  $MS$  technique. This scheme can be implemented in any modulation  $MS$  and improves the energy efficiency of low amplitude symbols as compared to traditional power splitting architecture based SWIPT ( $PS$ ). We studied the impact of CPs in EH using hybrid constellation shaping to improve the spectral efficiency. It was shown that,  $MS$  has better SER performance as compared to  $PS$ . It can also outperform  $PS$  in terms of achievable rates.

#### REFERENCES

- [1] D. N. K. Jayakody, J. Thompson, S. Chatzinotas, and S. Durrani, *Wireless Information and Power Transfer: A New Paradigm for Green Communications*. New York, NY, USA: Springer, 2017.
- [2] T. D. P. Perera, D. N. K. Jayakody, S. K. Sharma, S. Chatzinotas, and J. Li, "Simultaneous wireless information and power transfer (SWIPT): Recent advances and future challenges," *IEEE Commun. Surveys Tuts.*, vol. 20, no. 1, pp. 264–302, 1st Quart., 2018.
- [3] W. Liu, X. Zhou, S. Durrani, and P. Popovski, "SWIPT with practical modulation and RF energy harvesting sensitivity," in *Proc. IEEE Int. Conf. Commun. (ICC)*, Kuala Lumpur, Malaysia, May 2016, pp. 1–7.
- [4] J. G. Forney, R. G. Gallager, G. Lang, F. M. Longstaff, and S. U. Qureshi, "Efficient modulation for band-limited channels," *IEEE J. Sel. Areas Commun.*, vol. JSAC-2, no. 5, pp. 632–647, Sep. 1984.
- [5] F. R. Kschischang and S. Pasupathy, "Optimal nonuniform signaling for Gaussian channels," *IEEE Trans. Inf. Theory*, vol. 39, no. 3, pp. 913–929, May 1993.
- [6] W. Betts, A. R. Calderbank, and R. Laroia, "Performance of nonuniform constellations on the Gaussian channel," *IEEE Trans. Inf. Theory*, vol. 40, no. 5, pp. 1633–1638, Sep. 1994.
- [7] J.-X. Cai *et al.*, "70.4 Tb/s capacity over 7,600 km in C+L band using coded modulation with hybrid constellation shaping and nonlinearity compensation," in *Proc. Opt. Fiber Commun. Conf. Exhibit. (OFC)*, Los Angeles, CA, USA, Mar. 2017, pp. 1–3.
- [8] J. R. Barry, E. A. Lee, and D. G. Messerschmitt, *Digital Communication*. New York, NY, USA: Springer, 2012.
- [9] D. M. Arnold, H.-A. Loeliger, P. O. Vontobel, A. Kavcic, and W. Zeng, "Simulation-based computation of information rates for channels with memory," *IEEE Trans. Inf. Theory*, vol. 52, no. 8, pp. 3498–3508, Aug. 2006.
- [10] T. Fehenberger, A. Alvarado, G. Böcherer, and N. Hanik, "On probabilistic shaping of quadrature amplitude modulation for the nonlinear fiber channel," *J. Lightw. Technol.*, vol. 34, no. 21, pp. 5063–5073, Nov. 1, 2016.